Chemical Science

ROYAL SOCIETY OF CHEMISTRY

EDGE ARTICLE

View Article Online
View Journal | View Issue

Cite this: *Chem. Sci.*, 2025, **16**, 19867

All publication charges for this article have been paid for by the Royal Society of Chemistry

Efficient capture of trace benzene vapor by metal–organic frameworks modified with macrocyclic pyridyl ligands

Gang Liang,[a] De-Jian Chen,[a] Zhu-Jun Long,[a] Hao Zhuo,[b] Xiao-Feng Zhong,[b] Xiong-Hai Chen,[b] Huai-Yu Shao,[c] Zong-Wen Mo *[ad] and Xiao-Ming Chen[b]

The capture of trace benzene vapor is an important and huge challenge due to its serious toxicity. Physisorbents usually exhibit weak interactions especially in the presence of trace concentrations, thus possessing poor removal performance. Herein, an efficient post-synthetic modification strategy with various mono-, bi-, and tri-pyridyl derivative ligands was performed on the parent [$Fe_3(\mu_3$-O)(OH)$(H_2O)_2$(pet)] (**NU-1500(Fe)**, H_6pet = peripherally extended triptycene, 4,4′,4″,4‴,4⁗,4⁗′-(9,10-dihydro-9,10-[1,2]benzenoanthracene-2,3,6,7,14,15-hexayl)hexabenzoic acid) with large hexagonal pores (14 × 19 Å^2) and modifiable metal sites. Remarkably, these MOFs can regulate the performance of trace adsorption of benzene. Among them, the tri-pyridyl ligand modified [$Fe_3(\mu_3$-O)(pet)(tph)] (**WYU-107**, Htph = 2,5,8-tri-(4-pyridyl)-1,3,4,6,7,9-hexaazaphenalene) reaches an uptake of 6.21 mmol g^{-1} at 298 K and P/P_0 = 0.01 by virtue of the significant interactions between the pore partitioned host-framework and benzene molecules, which shows a capture performance exceeding that of most of the reported porous materials. At the same time, breakthrough experiments revealed that **WYU-107** can capture trace benzene in the air, and *in situ* variable-pressure PXRD indicates the reversible deformation behavior during the adsorption process. Theoretical calculations and *in situ* single-crystal structure reveal that the significant interactions are closely related to the insertion of the functional tph ligand, facilitating the capture of benzene vapor at trace levels.

Received 9th July 2025
Accepted 15th September 2025

DOI: 10.1039/d5sc05093f

rsc.li/chemical-science

Introduction

According to the World Health Organization, benzene is a highly toxic carcinogen, which seriously endangers human health even at trace levels.[1] Therefore, it is necessary to develop functional materials to realize efficient benzene vapor capture, especially at trace concentrations. Current methods to remove benzene vapor from indoor air include oxidation and adsorption by functional porous materials. However, high energy consumption and low adsorption efficiency (weak interactions between the host-framework and benzene molecules) limit the application.[2–6]

As a booming sort of porous material, metal–organic frameworks (MOFs) are well-known for their highly designable, tunable structures and pore surfaces, which play important roles in numerous applications,[7,8] such as gas storage/capture,[9] selective separation and molecular sensing.[10–12] Recently, a few MOFs have demonstrated huge potential in the removal of saturated benzene vapor even at trace levels. For example, the unique double-walled MOF, [Co(dpn)] (BUT-54(Co), H_2dpn = 2,7-di(1*H*-pyrazol-4-yl)naphthalene) achieved a benzene vapor uptake of 4.31 mmol g^{-1} at P/P_0 = 0.01 due to the multiple C–H···π interactions between dpn^{2-} ligands and benzene molecules.[11] Similarly, the benzene vapor uptake of [Al$(\mu$-O$)_2(\mu$-OH)(dbp)] (ZJU-520(Al), H_2dbp = 4,6-di(4-carboxyphenyl) pyrimidine) reaches 5.98 mmol g^{-1} at 298 K and P/P_0 = 0.01 based on the strong Al···π interactions between AlO_6 clusters and benzene molecules.[13] Besides, single-atom(Zn) sites in defective-MIL-125, [$Ti_8O_8(\mu$-OH$)_4$(bdc$)_6$] (H_2bdc = 1,4-benzenedicarboxylic acid), can serve as potential sites toward benzene molecules, achieving the record high benzene uptake (7.63 mmol g^{-1}) at 298 K and 1.2 mbar.[14] These results clearly demonstrate that enhancing the interaction between the host-framework and benzene molecules is the key to achieving efficient capture of benzene vapor.[15,16] Despite the progress in trace adsorption of benzene vapor, the efficient capture based on directional assembly remains a huge challenge. In principle, the introduction of aromatic macrocyclic groups into MOF frameworks is an effective approach to improve the adsorption of

[a]*School of Environmental and Chemical Engineering, Wuyi University, Jiangmen, Guangdong 529020, China. E-mail: wyuchemmzw@126.com*

[b]*MOE Key Laboratory of Bioinorganic and Synthetic Chemistry, GBRCE for Functional Molecular Engineering, School of Chemistry, IGCME, Sun Yat-Sen University, Guangzhou 510275, China*

[c]*Joint Key Laboratory of the Ministry of Education, Institute of Applied Physics and Materials Engineering, University of Macau, Macau SAR, China*

[d]*Guangdong Provincial Laboratory, Fine Chemical Engineering Jie Yang Center, China*

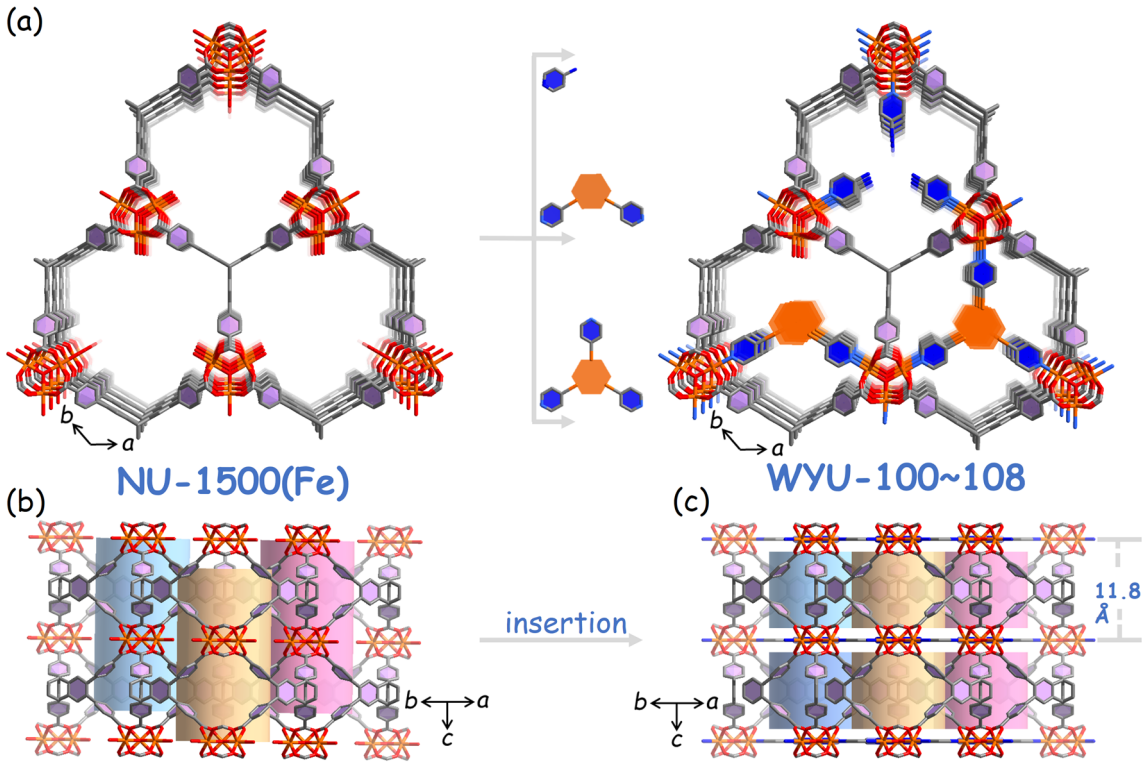

Fig. 1 (a) The post-modification strategy of various pyridyl derivative ligands based on the prototype **NU-1500(Fe)**. The comparison of pore void between (b) **NU-1500(Fe)** and (c) post-modification **WYU-107**.

benzene vapor by virtue of the strong interaction between aromatic macrocyclic ligands and benzene molecules. For example, $[Sr_2(bindi)(DMF)(H_2O)]$ (**WYU-61**, H_4bindi = *N*,*N*′-bis(5-isophthalic acid)-naphthalenediimide, DMF = *N*,*N*-dimethylformamide), a MOF with aromatic macrocyclic bindi ligands, exhibits the unique "bilateral π–π stacking" host–guest interaction between benzene molecules and the macrocyclic ligands, realizing the adsorption and detection of trace benzene vapor.[17] However, the poor solubility of macrocyclic derivative ligands and unpredictability of the direct synthetic method, as well as the low porosity of host-frameworks lead to difficulty in orientated construction of MOFs. In contrast, the insertion of aromatic macrocyclic ligands into the parent MOFs by post-synthetic modification (PSM) is an effective strategy, and the key is the compatibility of the parent MOFs and inserted ligands.[18–21]

Here, we report a series of MOFs (**WYU-100–108**, WYU = Wuyi University), synthesized by PSM of $[Fe_3(\mu_3\text{-}O)(OH)(H_2O)_2(pet)]$ (**NU-1500(Fe)**),[22] H_6pet = peripherally extended triptycene, 4,4′,4″,4‴,4⁗,4⁗′-(9,10-dihydro-9,10-[1,2]benzenoanthracene-2,3,6,7,14,15-hexayl)hexabenzoic acid) with large hexagonal pores (14 × 19 Å^2) and various modifiable metal sites for insertion of various pyridyl ligands (Fig. 1a).

Interestingly, the insertion is not only feasible for smaller mono-pyridyl derivative ligands but also for bi-pyridyl derivative ligands, and even for larger tri-pyridyl derivative ligands, compared with the limited porosity MOFs, such as $[Zr_6(\mu_3\text{-}O)_4(\mu_3\text{-}OH)_4(OH)_4(H_2O)_4(ettc)_2]$ (WSU-5, H_4ettc = 4′,4‴,4⁗′,4⁗″-(ethene-1,1,2,2-tetrayl)tetrakis([1,1′-biphenyl]-4-carboxylic acid)) and $Zr_6(\mu_3\text{-}O)_4(\mu_3\text{-}OH)_4(HCOO)_4(tcpe)_2$ (H_4tcpe = 1,1,2,2-tetra(4-carboxylphenyl)ethylene).[23,24] The saturation uptake of benzene vapor, stepped pressure, and the trace adsorption can be regulated by the insertion of different types of pyridyl derivative ligands based on the various host–guest interactions. Notably, $[Fe_3(\mu_3\text{-}O)(pet)(tph)]$ (**WYU-107**) containing the tri-pyridyl derivative ligand 2,5,8-tri-(4-pyridyl)-1,3,4,6,7,9-hexaazaphenalene (Htph) achieves an exceptional benzene uptake of 6.21 mmol g^{-1} by virtue of the strong interactions between the larger conjugated hexaazaphenalene-based ligand and benzene molecules at $P/P_0 = 0.01$, which is three times that of the parent **NU-1500(Fe)** (2.12 mmol g^{-1}).[25] As far as we know, **WYU-107** is the first post-synthetic modified MOF showing highly efficient capture of benzene vapor at trace levels, being superior to most of the reported porous materials, and only next to the defective-MIL-125-X (X = Mn, Co, Ni, Cu, Zn). Furthermore, breakthrough experiments further demonstrate that **WYU-107** has excellent potential for trace benzene capture. The combination of *in situ* single-crystal X-ray diffraction (SCXRD) and theoretical calculations demonstrates that the large aromatic tph ligand is conducive to the benzene vapor adsorption under low pressure.

Results and discussion

NU-1500(Fe) with **acs** topology is constructed from pet ligands and trinuclear $[Fe_3(\mu_3\text{-}O)(H_2O)_2(OH)(RCOO)_6]$ clusters. There are large hexagonal channels (14 × 19 Å^2) in the framework

along the *c*-axis, and the pore ratio reaches 74.8%. More importantly, there are two terminal H_2O and one OH^- ligands in the cluster, which can serve as perfect sites for ligand replacement by PSM. On the other hand, the compatibility of the substituting ligand and the spatial arrangement of the modifiable sites are also significant factors. Compared to **NU-1500(Fe)**, other parent MOFs, such as $[Co_2(dobdc)]$ (MOF-74(Co), H_4dobdc = 2,5-dihydroxyl-1,4-benzenedicarboxylic acid,[26] $[Fe_3(\mu_3\text{-}O)(tba)_3(OH)(H_2O)_2]$ (MIL-88A(Fe), H_2tba = *trans*-2-butenedioic acid) and $[Zr_{12}(\mu\text{-}O)_8(\mu\text{-}OH)_8(CH_3COO)_{12}(\text{-tcpb-}Br_2)_3]$ (NU-600, H_4tcpb-Br_2 = 4-dibromo-2,3,5,6-tetrakis(4-carboxyphenyl)benzene), exhibit more restricted pore sizes and modifiable sites. Their inherent limitations hinder accommodation of the extended or bulky organic ligands.[27,28] As far as we know, few MOFs can achieve various types of ligand insertion, not to mention macrocyclic ligands with large molecular sizes. Fortunately, the combination of large pore size and three modifiable sites in the parent **NU-1500(Fe)** allows for modifications of not only smaller mono-pyridyl derivative ligands but also larger bi-pyridyl and even tri-pyridyl derivative ligands (Fig. S1). In principle, the insertion is feasible as long as the ligand length of L_1 (mono-pyridyl ligand) is shorter than the pore size, or the shapes and sizes of L_2 (bi-pyridyl ligand) and L_3 (tri-pyridyl ligand) are adaptable to two and three modifiable sites, respectively (Fig. S2).

The PSM strategy was proved by single-crystal X-ray diffraction (SCXRD) (Tables S2–S5), as well as ^{1}H NMR spectra. The ratio of H_6pet : L_1 (apy, ina, pyb) is close to 1 : 3 (Fig. S3–S5), suggesting that the three terminal H_2O/OH^- ligands in a $[Fe_3(\mu_3\text{-}O)(H_2O)_2(OH)(RCOO)_6]$ cluster can be replaced by mono-pyridyl ligands to give the corresponding modified $[Fe_3(\mu_3\text{-}O)(apy)_3(pet)]$ *x* (**WYU-100**, apy = 4-aminopyridine, *x* = counter anions), which crystallizes in the hexagonal *P*6*m*2 space group. There are three apy ligands inserted into each trinuclear cluster of the parent **NU-1500(Fe)** since the length of the ligand (4.6 Å) is less than d_1 (Fig. S2). Furthermore, similar mono-pyridyl ligands (ina = isonicotinic acid, pyb = pyridine-4-boronic acid) can also be used to modify **NU-1500(Fe)** into $[Fe_3(\mu_3\text{-}O)(ina)_3(pet)]$ *x* (**WYU-101**) and $[Fe_3(\mu_3\text{-}O)(pyb)_3(pet)]$ *x* **(WYU-102)**, respectively. However, the orientations of apy and ina ligands in the frameworks of **WYU-100** and **WYU-101** are vertical, while that of the pyb ligand in **WYU-102** is parallel, to the trinuclear core (Fig. S12).

Considering the distribution of trinuclear clusters in the hexagonal pore, bi-pyridyl ligands with the length close to 12.6 Å (the distance between two Fe^{3+} ions in adjacent trinuclear clusters, Fig. S2) can also modify **NU-1500(Fe)**. The larger N^1,N^3-di(pyridine-4-yl)isophthalamide (bpipa) ligand with functional amide groups was then inserted into it to furnish a new MOF, $[Fe_3(\mu_3\text{-}O)(OH)(pet)(bpipa)]$ (**WYU-103**). The ratio of H_6pet : L_2 (L_2 = bpipa, dpyc, or dpyn) is close to 1 : 1 based on ^{1}H NMR spectra measurements (Fig. S6–S8), suggesting that two terminal H_2O molecules in each trinuclear cluster can be replaced by pyridyl derivative ligands, transforming the 6-connected **NU-1500(Fe)** into the 8-connected **WYU-103**. Consequently, the hexagonal channel is partitioned into two smaller ones.[15] Similarly, other bi-pyridyl ligands featuring larger bending angles (103.5°) and longer lengths (11.95 Å), such as 3,6-di(pyridin-4-yl)-9*H*-carbazole (dpyc) and 2,7-di(4-pyridyl) naphthalene (dpyn), can also facilitate the assembly of similar 8-connected $[Fe_3(\mu_3\text{-}O)(OH)(pet)(dpyc)]$ (**WYU-104**) and $[Fe_3(\mu_3\text{-}O)(OH)(pet)(dpyn)]$ (**WYU-105**). These results further demonstrate the high adaptability of **NU-1500(Fe)** to diverse ligand modifications.

Based on the above results, PSMs with larger tri-pyridyl derivative ligands (tpybtc = *N*,*N*′,*N*″-tris(4-pyridinyl)-1,3,5-benzenetricarboxamide, Htph = (2,5,8-tri-(4-pyridyl)-1,3,4,6,7,9-hexaazaphenalene, tpvb = 1,3,5-tris((*E*)-2-(pyridin-4-yl)vinyl)benzene) were further performed to verify the feasibility of this strategy.[29] SCXRD reveals that three terminal H_2O/OH^- ligands on the trinuclear cluster can be completely replaced by the tri-pyridyl ligands to achieve 9-connected MOFs, $[Fe_3(\mu_3\text{-}O)(pet)(tpybtc)]$ *x* **(WYU-106)**, $[Fe_3(\mu_3\text{-}O)(pet)(tph)]$ **(WYU-107)** and $[Fe_3(\mu_3\text{-}O)(pet)(tpvb)]$ *x* **(WYU-108)**. ^{1}H NMR spectral measurements further verified that the ratio of H_6pet : L_3 (L_3 = tpybtc, tph, tpvb) is close to 1 : 1 (Fig. S9–S11). The replaced groups in the ligands derived from **WYU-106–108** were further confirmed by FT-IR spectra (Fig. S15). As the terminal OH^- ligand is replaced by the deprotonated tph ligand, **WYU-107** becomes a neutral framework. In contrast, there are counter anions accommodated in **WYU-106** and **WYU-108**, although these anions cannot be clearly determined by SCXRD due to their serious disorder. Interestingly, the symmetries of **WYU-106–108** are maintained after the ligand insertion of tpybtc, Htph and tpvb due to the geometric compatibility of the ligands and the rigidity of the parent framework. It is worth noting that the large 3D pore in **NU-1500(Fe)** is partitioned into three smaller ones after the above modification. Notably, the porosity decreased from 74.8% of **NU-1500(Fe)** to 69% of **WYU-100–102** with mono-pyridyl ligands, to 67% of **WYU-103–105** with bi-pyridyl ligands, and finally to 66% of **WYU-106–108** with tri-pyridyl ligands. More importantly, the functional N and O sites are successfully introduced into the host-framework upon modification. For example, the anionic tph ligand contains a large hexaazaphenalene moiety with six nitrogen atoms, which is conducive to the formation of multiple hydrogen bonds between the macrocycle moiety and guest molecules. In other words, various types of pyridyl ligands can be inserted into the host-framework to regulate the functionality.

The purities of as-synthesized **NU-1500(Fe)** and **WYU-100–108** were checked by powder X-ray diffraction (PXRD) patterns, which are consistent with the simulated ones, indicating the high purity and crystallinity (Fig. S13 and S14). TG curves of as-synthesized **WYU-100–108** showed large weight loss from room temperature to 350 °C due to the removal of the free guest and coordination solvent molecules within the pore, and the remaining host framework decomposed above 400 °C (Fig. S16 and S17). The porosities of **WYU-100–108** were measured by N_2 sorption isotherms at 77 K, which showed typical type-I curves (Fig. 2a). The adsorption capacities of these frameworks are lower than those of the parent **NU-1500(Fe)** attributed to the insertion of various ligands. Specifically, the pore volumes of **NU-1500(Fe)**, **WYU-100**, **WYU-105** and **WYU-107** can be calculated to be 1.25, 1.07, 0.99 and 0.93 $cm^3\ g^{-1}$, respectively, which

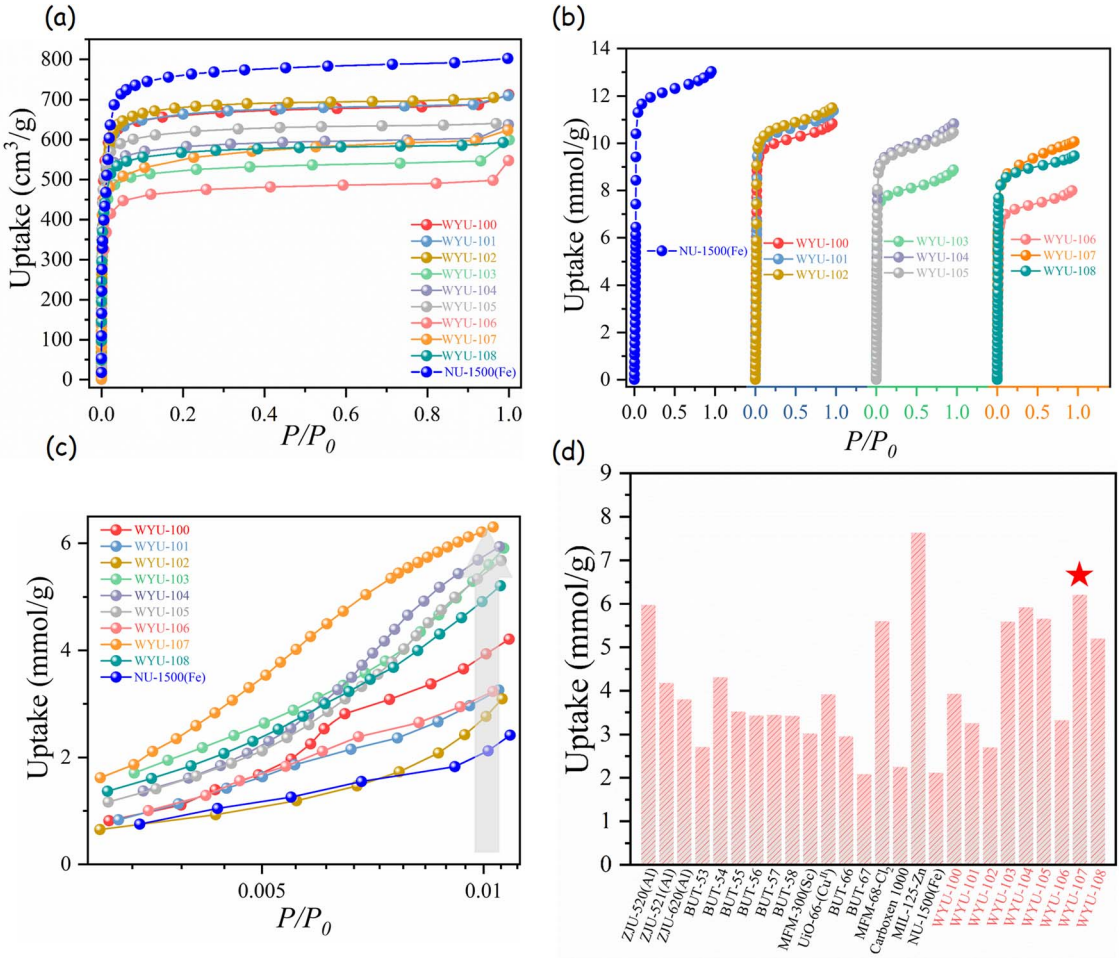

Fig. 2 (a) N_2 sorption isotherms at 77 K and (b) benzene vapor adsorption isotherms at 298 K for **WYU-100–108** and **NU-1500(Fe)**. (c) Logarithmic-scale plots of $P/P_0 = 0.01$ to view the adsorption of benzene at low partial pressures. (d) The performance comparison of trace benzene vapor uptakes for various MOFs at $P/P_0 = 0.01$.

are close to their theoretical values (1.40, 1.19, 1.13 and 0.97 $cm^3\ g^{-1}$). Fitting the adsorption isotherms of **NU-1500(Fe)**, **WYU-100**, **WYU-105** and **WYU-107** using the Brunauer–Emmett–Teller (BET) model gave the surface areas of 2900, 2690, 2480 and 2070 $m^2\ g^{-1}$, respectively. As expected, the insertion of different sized ligands (L_1 to L_3) can regulate the pore size of the host-framework.

Nonlocal Density Functional Theory (NLDFT) calculations gave a broad pore size distribution centered from 8.3 to 12 Å (Fig. S18), which is smaller than that of the parent **NU-1500(Fe)** (14 Å) due to the insertion of various pyridyl ligands. Interestingly, the pore window of **WYU-107** was partitioned into three triangular channels (7.8 × 6.9 $Å^2$), being consistent with the value from the pore size distribution. This pore size compatibility with molecules significantly promotes the host–guest interaction, which is conducive to improving the capture performance. In addition, these MOFs retain their frameworks after being exposed to air or immersed in aqueous solutions in a wide pH range from 3 to 10 for one year (Fig. S19–S21). Moreover, ^1H NMR measurement of **WYU-100–108** after post-treatment (the desorbed MOFs were exposed to air for one year, and washed with DMF and acetone for several times) further verified the stability of the inserted pyridyl ligand (Fig. S3–S11). However, 77 K N_2 adsorption measurements of **WYU-100–108** after being exposed to air for one year revealed a decline in saturation uptake. Among them, the uptake of tri-pyridyl modified MOFs (**WYU-107** and **WYU-108**) displayed a marginally smaller decline than bi-pyridyl and mono-pyridyl modified MOFs (Fig. S22). This trend was further corroborated by the result obtained from **WYU-107** after immersion at pH = 3 and pH = 10. These observations can be attributed to the higher structural connectivity, which is more conducive to the stability of the framework (Fig. S23).

As the pore sizes and functional ligands inserted in the host-framework have a significant impact on the host–guest interactions, benzene vapor sorption isotherms at 298 K were measured, which showed typical type-I curves (Fig. 2b) and verified the significant interaction between the guest benzene and host-framework. Obviously, the saturated benzene adsorption capacities of **WYU-MOF** correlate with pore volumes, as well as the pore sizes, whose capacity order gradually decreases from mono-pyridyl to tri-pyridyl ligand insertion with

increase in the size of the pyridyl ligand. Specifically, the uptakes of mono-pyridyl ligand modified **WYU-100** (10.83 mmol g^{-1}), **WYU-101** (11.37 mmol g^{-1}) and **WYU-102** (11.50 mmol g^{-1}) are lower than that of the parent **NU-1500(Fe)** (13.02 mmol g^{-1}), due to the reduction of pore volume after the insertion of mono-pyridyl ligands. Similarly, the uptakes of bi-pyridyl ligand modified **WYU-104** (10.50 mmol g^{-1}) and **WYU-105** (10.46 mmol g^{-1}) are higher than those of tri-pyridyl ligands modified **WYU-107** (10.07 mmol g^{-1}) and **WYU-108** (9.47 mmol g^{-1}). It is worth noting that MOFs modified with ligands of amide groups, **WYU-103** (8.88 mmol g^{-1}) and **WYU-106** (7.99 mmol g^{-1}), exhibit poor benzene vapor uptakes, probably because the charge density and distribution of ligand are not conducive to interacting with the benzene molecule. The saturation uptakes of **WYU-100–108** are not superior compared to those of the reported MOFs, $[Zn_{12}(\mu\text{-}O)_3(BTB)_4(MPTDC)_9]$ (NENU-513, H_3BTB = benzene-1,3,5-tribenzoic acid, H_2MPTDC = 3-methyl-4-phenylthieno[2,3-*b*]thiophene-2,5-dicarboxylic acid) (21.62 mmol g^{-1}), MIL-101(Cr) (15.84 mmol g^{-1}) and ZJU-520 (12.07 mmol g^{-1}) (Table S1).[13,30,31]

Interestingly, further analysis shows that the frameworks modified with various pyridyl ligands exhibit exceptional benzene adsorption behaviors at relatively low pressures. Specifically, **WYU-100–108** exhibit significantly steep increases at low pressures, indicating the great potential for the capture of benzene vapor at trace levels. According to the literature, the capture of benzene at low concentrations, especially at low pressure (P/P_0 < 0.01), is critically important as it directly correlates with the challenging scenario of adsorption of highly diluted pollutants from air.[11,32–34] This value corresponds to a partial benzene pressure of ~127 Pa, and equates to a benzene concentration of approximately 1250 ppm. Although benzene is present in polluted air or industrial settings at concentrations of parts-per-billion (ppb) and lower levels (parts-per-million (ppm)), P/P_0 = 0.01 is usually used to simulate the trace conditions in the laboratory for investigating the capture performance of benzene.

For example, **WYU-100**, **WYU-101** and **WYU-102** show benzene uptakes of 3.93, 3.25 and 2.76 mmol g^{-1} at $P/P_0 = 0.01$, respectively, which are significantly higher than that (2.12 mmol g^{-1}) of their parent **NU-1500(Fe)**. At the same time, those of **WYU-103**, **WYU-104** and **WYU-105** are 5.59, 5.92 and 5.66 mmol g^{-1}, respectively, while those of **WYU-106**, **WYU-107** and **WYU-108** reach 3.23 mmol g^{-1}, 6.21 mmol g^{-1} and 5.20 mmol g^{-1}, respectively (Fig. 2c). Notably, the uptake of **WYU-107** modified with tph ligand is about three times higher than that of **NU-1500(Fe)**. As far as we know, the trace adsorption capacity of **WYU-107** exceeds that of most porous materials, and is only below that of the defective-MIL-125-X (7.63 mmol g^{-1}, X = Mn, Co, Ni, Cu, Zn) (Fig. 2d).[11,13,31,33–35] In short, the pore volume is conducive to the saturation uptake of benzene, while the adsorption performance of trace benzene uptake is related to the sizes and structures of the inserted ligands in the framework, which govern the host–guest interaction. Consequently, the uptakes of trace benzene vapor gradually increase from mono-pyridyl **WYU-100** to bi-pyridyl **WYU-105** to tri-pyridyl **WYU-107**. In addition, the benzene vapor uptake for **WYU-107** showed negligible decline after multiple cycles, suggesting the significant reproducibility for **WYU-107** (Fig. S24). In order to verify the structural distortions of the framework during the adsorption process, *in situ* variable-pressure PXRD spectra of activated **WYU-107** were collected, which show that a new diffraction peak (the highlighted zone) occurred with the pressure increase of benzene vapor. At the same time, the PXRD pattern of desorption at 120 °C was consistent with that of as-synthesized **WYU-107**, which may be attributed to the deformation behaviour during the adsorption process (Fig. 3a).

To evaluate the efficiency of **WYU-107** for the capture of trace benzene at different humidity levels (RH = 0% and 40%), dynamic breakthrough experiments of **WYU-107** were performed. The results indicated that benzene vapor started to breakthrough the column of ~3750 min g^{-1} under dry conditions (RH = 0%), corresponding to a dynamic adsorption capacity of 6.64 mmol g^{-1}. However, the adsorption capacity reduced to 1.22 mmol g^{-1} (~652 min g^{-1}) under the humidity level (RH) of 40% due to the competitive adsorption of water (Fig. 3b and S25–S26). At the same time, adsorption kinetic experiments of benzene vapor were performed on **WYU-100**, **WYU-105** and **WYU-107** as examples at $P/P_0 = 0.01$. The results show that there were 12 minutes more for adsorption equilibrium to be reach in the case of **WYU-100**, while there were only 2 minutes for **WYU-107** in the case of the macrocyclic ligands. Meanwhile, the adsorption uptake (5.90 mmol g^{-1}) of **WYU-107** is close to the value (6.21 mmol g^{-1}) from the adsorption isotherm at $P/P_0 = 0.01$. These results indicate that the PSM of macrocyclic ligands into **NU-1500(Fe)** can significantly enhance the host–guest interaction, which is conducive to the enhanced rate of adsorption of benzene vapor (Fig. S27).

To gain insight into the interaction mechanism between the framework of **WYU-107** and benzene molecules, **C_6H_6@WYU-107** was characterized by SCXRD, showing clearly the positions of benzene molecules in the pores (Fig. 4). There are three binding sites (I, II and III) for C_6H_6 in **C_6H_6@WYU-107**. Specifically, sites I and II are located in the cavities enclosed by a pair of triptycence moieties and a pair of trinuclear clusters, respectively. The benzene molecule in site I is bound to the triptycence moieties through C–H$\cdots\pi$ interactions (d = 3.7 to 4.4 Å), while that in site II is stabilized by C–H$\cdots\pi$ interactions (d = 4.2–4.5 Å),[36–39] as well as strong C–H$\cdots$O interactions with carboxylate groups (2.9–3.3 Å). Notably, a pair of benzene molecules are tightly encapsulated in site III enclosed by a pair of tph ligands, where each benzene molecule simultaneously interacts with the hexaazaphenalene moiety in a face-to-face fashion at a short distance of *ca.* 3.4 Å and with the other benzene molecule at a distance of *ca.* 4.8 Å through special π–π stacking interactions.[40] Such strong host–guest interactions obviously contribute to the remarkable benzene uptake of **WYU-107** at low pressures compared to the parent **NU-1500(Fe)**, demonstrating the crucial role of macrocyclic tph in enhancing the binding interactions with benzene molecules. At the same time, the results of theoretical calculations for **C_6H_6@WYU-107** and **NU-1500(Fe)** demonstrate that the interaction sites are in substantial accordance with the *in situ* SCXRD.[41–43]

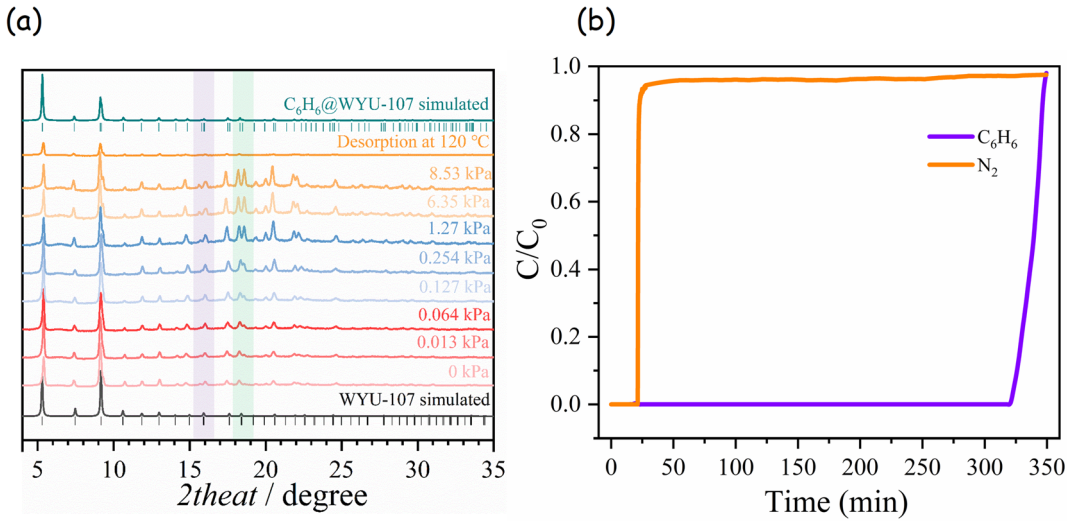

Fig. 3 (a) *In situ* variable-pressure PXRD patterns of **WYU-107**, collected under benzene vapor pressure from 0 to 8.53 kPa (guest-free to C_6H_6@**WYU-107**) and desorption at 120 °C after the adsorption process. (b) Benzene breakthrough curves for **WYU-107** in air at 298 K.

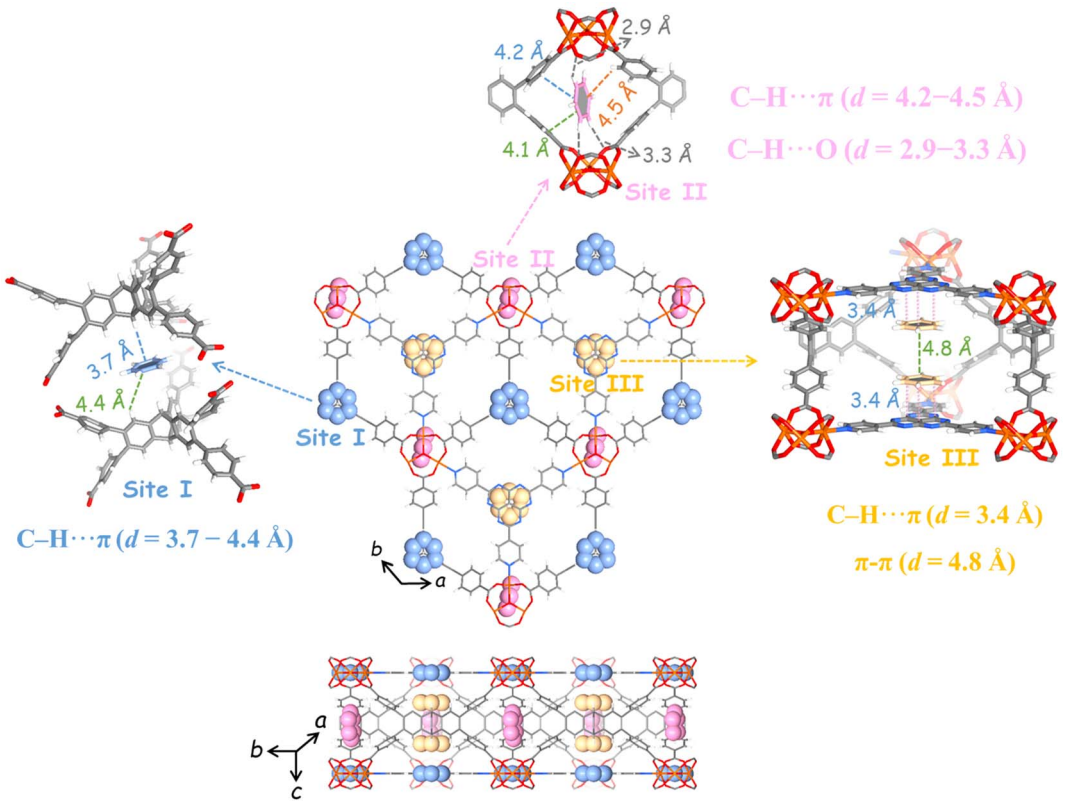

Fig. 4 The adsorption sites of C_6H_6@**WYU-107** characterized by single-crystal X-ray diffraction.

Furthermore, the calculations of electrostatic potential (ESP) indicated that there are significant dispersion forces between benzene molecules and multiple adjacent atoms within the host-framework at site I, due to the close distances, while strong induction and orientation forces were present at site II due to the electrostatic interaction between hydrogen atoms (positive charge) of benzene and oxygen atoms (negative charge) of carboxylate groups. Specifically, the calculated binding energy of the benzene molecule in the parent **NU-1500(Fe)** at site II is -58.01 kJ mol^{-1}, which is slightly higher than that at site I of -57.23 kJ mol^{-1} (Fig. 5a and b). In contrast, **WYU-107** possesses not only two adsorption sites (site I and II) similar to those of **NU-1500(Fe)**, with the calculated binding energies being -46.40 kJ mol^{-1} and -71.78 kJ mol^{-1} (Fig. 5c and d), respectively, but

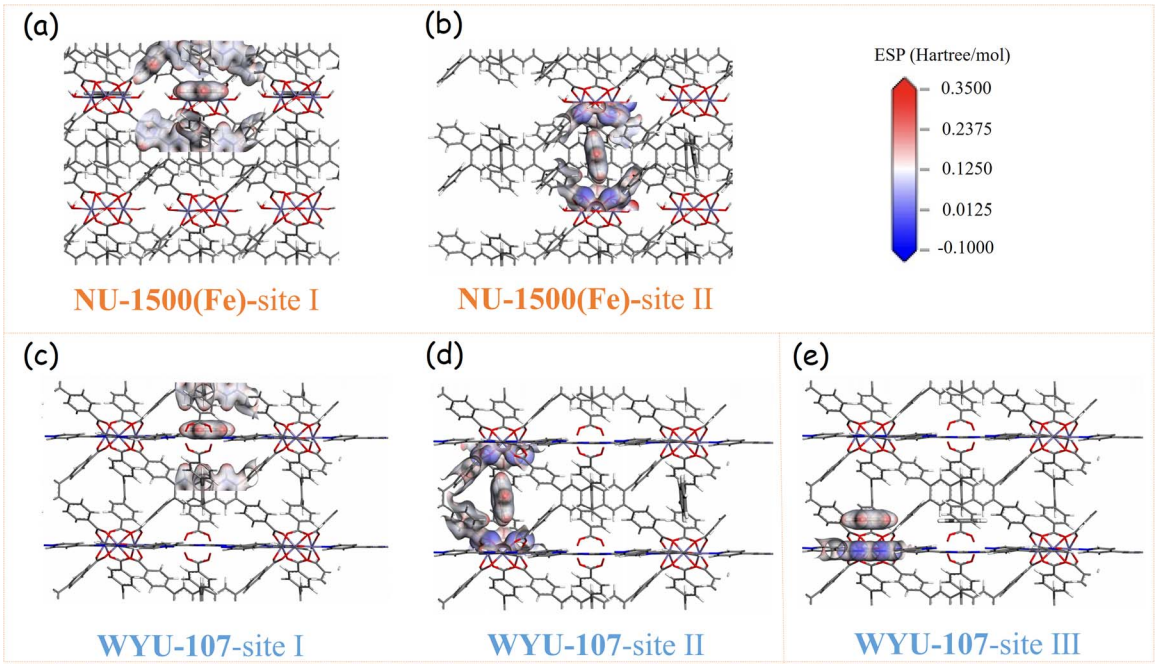

Fig. 5 The ESP of adsorption binding sites in **NU-1500(Fe)** (a and b) and **WYU-107** (c–e).

also an additional site III with a calculated binding energy of −33.71 kJ mol^{-1} (Fig. 5e). In other words, the insertion of macrocyclic ligands induces structural deformation, resulting in the enhancement of host–guest interactions at site II, and introducing an extra site III in **WYU-107** at the same time. Consequently, such multiple effects result in the significantly enhanced capture of trace benzene.

Conclusions

In summary, various pyridyl derivative ligands were successfully integrated into **NU-1500(Fe)** by a post-synthetic modification strategy, allowing the regulation of host–guest interaction. Particularly, **WYU-107** modified with a tri-pyridyl ligand of functional macrocyclic moiety exhibits significant interaction for benzene molecules by virtue of the combination of π–π, C–H···π and C–H···O interactions, enabling the capture performance surpassing most reported porous materials. These results demonstrate that the enhancement of the host–guest interactions by post-synthetic modification of functional macrocyclic ligand insertion in large pores of MOFs is effective for the capture of trace benzene vapor, which may inspire the molecular design of porous materials to achieve higher capture efficiency.

Author contributions

Gang Liang: investigation, data curation, writing – original draft. De-Jian Chen: methodology, data curation, resources. Zhu-Jun Long: methodology, data curation, resources. Hao Zhou: resources, methodology. Xiao-Feng Zhong, Xiong-Hai Chen and Huai-Yu Shao: review & editing. Zong-Wen Mo: project administration, funding acquisition, writing – original draft, writing – review & editing, formal analysis. Xiao-Ming Chen: supervision, project administration, funding acquisition.

Conflicts of interest

The authors declare no competing financial interest.

Data availability

The data that support the findings of this study are available from the corresponding author upon reasonable request.

CCDC 2424097–2424106 contain the supplementary crystallographic data for this paper.[44a–j]

Supplementary information: Experimental details , theoretical calculation methods, PXRD patterns, thermogravimetric analysis (TGA) data, and crystallographic data (PDF). See DOI: **https://doi.org/10.1039/d5sc05093f**.

Acknowledgements

This work was supported by the Hong Kong–Macao Joint Research and Development Fund of Wuyi University (2022WGALH06), and NSFC (22090061). We also thank Ze Chang (Nankai University), Rui-Biao Lin and Wen-Bin Li (Sun Yat-Sen University) for their assistance with *in situ* PXRD and breakthrough test.

Notes and references

1 Y. Han, D. Brooks, M. He, Y. Chen, W. Huang, B. Tang, *et al.*, Enhanced Benzene Adsorption in Chloro-Functionalized

Metal-Organic Frameworks, *J. Am. Chem. Soc.*, 2024, **146**, 28080–28087.
2 T. N. Tu, T. M. Pham, Q. H. Nguyen, N. T. Tran, V. N. Le, L. H. Ngo, K. Chang and J. Kim, Metal-organic frameworks for aromatic-based VOC capture, *Sep. Purif. Technol.*, 2024, **333**, 125883.
3 X. Li, L. Zhang, Z. Yang, P. Wang, Y. Yan and J. Ran, Adsorption materials for volatile organic compounds (VOCs) and the key factors for VOCs adsorption process: A review, *Sep. Purif. Technol.*, 2020, **235**, 116213.
4 C. Lai, Z. Wang, L. Qin, Y. Fu, B. Li, M. Zhang, *et al.*, Metal-organic frameworks as burgeoning materials for the capture and sensing of indoor VOCs and radon gases, *Coord. Chem. Rew.*, 2021, **427**, 213565.
5 R. C. Zhao, L. H. Xie, X. M. Liu, Z. Liu, X. Y. Li and J. R. Li, Removal of Trace Benzene from Cyclohexane Using a MOF Molecular Sieve, *J. Am. Chem. Soc.*, 2024, **147**, 2467–2475.
6 L. Hu, M. Zhang, W. Wang, J. Hu, W. Wu, D. Lin and K. Yang, A Novel Mesoporous Aluminum-Based MOF with Large Pore Volume for High Concentration Benzene Adsorption, *Adv. Funct. Mater.*, 2025, **35**, 2425429.
7 O. I. F. Chen, C. H. Liu, K. Wang, E. Borrego Marin, H. Li, A. H. Alawadhi, J. A. R. Navarro and O. M. Yaghi, Water-Enhanced Direct Air Capture of Carbon Dioxide in Metal-Organic Frameworks, *J. Am. Chem. Soc.*, 2024, **146**, 2835–2844.
8 D. Sengupta, S. Bose, X. Wang, N. M. Schweitzer, C. D. Malliakas, H. Xie, *et al.*, Integrated CO_2 Capture and Conversion by a Robust Cu(I)-Based Metal–Organic Framework, *J. Am. Chem. Soc.*, 2024, **146**, 27006–27013.
9 H. Li, K. Wang, Y. Sun, C. T. Lollar, J. Li and H.-C. Zhou, Recent advances in gas storage and separation using metal–organic frameworks, *Mater. Today*, 2018, **21**, 108–121.
10 H. L. Zheng, J. Q. Zhao, Y. Y. Sun, A. A. Zhang, Y. J. Cheng, L. He, X. Bu, J. Zhang and Q. Lin, Multilevel-Regulated Metal–Organic Framework Platform Integrating Pore Space Partition and Open-Metal Sites for Enhanced CO_2 Photoreduction to CO with Nearly 100% Selectivity, *J. Am. Chem. Soc.*, 2023, **145**, 27728–27739.
11 T. He, X. J. Kong, Z. X. Bian, Y. Z. Zhang, G. R. Si, L. H. Xie, *et al.*, Trace removal of benzene vapour using double-walled metal–dipyrazolate frameworks, *Nat. Mater.*, 2022, **21**, 689–695.
12 C. Gu, N. Hosono, J. J. Zheng, Y. Sato, S. Kusaka, S. Sakaki and S. Kitagawa, Design and control of gas diffusion process in a nanoporous soft crystal, *Science*, 2019, **363**, 387–391.
13 L. Hu, W. Wu, M. Hu, L. Jiang, D. Lin, J. Wu and K. Yang, Double-walled Al-based MOF with large microporous specific surface area for trace benzene adsorption, *Nat. Commun.*, 2024, **15**, 3204.
14 Y. Han, W. Huang, M. He, B. An, Y. Chen, X. Han, *et al.*, Trace benzene capture by decoration of structural defects in metal–organic framework materials, *Nat. Mater.*, 2024, **23**, 1531–1538.
15 Z. H. Qiu, J. H. Li, B. X. He, P. Q. Liao, M. Y. Zhou, P. X. Li, R. B. Lin, J. P. Zhang and X. M. Chen, Fast adsorption and kinetic separation of benzene and cyclohexane/cyclohexene in a microporous metal azolate framework, *J. Mater. Chem. A*, 2024, **12**, 13240–13246.
16 X. Zhao, Y. Wang, D. S. Li, X. Bu and P. Feng, Metal–Organic Frameworks for Separation, *Adv. Mater.*, 2018, **30**, 1705189.
17 W. B. Li, Y. Wu, X. F. Zhong, X. H. Chen, G. Liang, J. W. Ye, Z. W. Mo and X. M. Chen, Fluorescence Enhancement of a Metal-Organic Framework for Ultra-Efficient Detection of Trace Benzene Vapor, *Angew. Chem., Int. Ed.*, 2023, **62**, e202303500.
18 C. X. Chen, Z. W. Wei, J. J. Jiang, S. P. Zheng, H. P. Wang, Q. F. Qiu, C. C. Cao, D. Fenske and C. Y. Su, Dynamic Spacer Installation for Multirole Metal–Organic Frameworks: A New Direction toward Multifunctional MOFs Achieving Ultrahigh Methane Storage Working Capacity, *J. Am. Chem. Soc.*, 2017, **139**, 6034–6037.
19 Y. Hu, X. Zhang, R. S. H. Khoo, C. Fiankor, X. Zhang and J. Zhang, Stepwise Assembly of Quinary Multivariate Metal-Organic Frameworks via Diversified Linker Exchange and Installation, *J. Am. Chem. Soc.*, 2023, **145**, 13929–13937.
20 O. I. F. Chen, C. H. Liu, K. Wang, E. Borrego Marin, H. Li, A. H. Alawadhi, J. A. R. Navarro and O. M. Yaghi, Water-Enhanced Direct Air Capture of Carbon Dioxide in Metal–Organic Frameworks, *J. Am. Chem. Soc.*, 2024, **146**, 2835–2844.
21 B. Li, D. Ma, Y. Li, Y. Zhang, G. Li, Z. Shi, S. Feng, M. J. Zaworotko and S. Ma, Dual Functionalized Cages in Metal–Organic Frameworks via Stepwise Postsynthetic Modification, *Chem. Mater.*, 2016, **28**, 4781–4786.
22 Z. Chen, P. Li, X. Zhang, P. Li, M. C. Wasson, T. Islamoglu, J. F. Stoddart and O. K. Farha, Reticular Access to Highly Porous acs-MOFs with Rigid Trigonal Prismatic Linkers for Water Sorption, *J. Am. Chem. Soc.*, 2019, **141**, 2900–2905.
23 S.-S. Meng, M. Xu, H. Guan, C. Chen, P. Cai, B. Dong, *et al.*, Anisotropic flexibility and rigidification in a TPE-based Zr-MOFs with scu topology, *Nat. Commun.*, 2023, **14**, 5347.
24 M. J. Hurlock, L. Hao, K. W. Kriegsman, X. Guo, M. O'Keeffe and Q. Zhang, Evolution of 14-Connected Zr_6 Secondary Building Units through Postsynthetic Linker Incorporation, *ACS Appl. Mater. Interfaces*, 2021, **13**, 51945–51953.
25 A. N. Hong, E. Kusumoputro, Y. Wang, H. Yang, Y. Chen, X. Bu and P. Feng, Simultaneous Control of Pore-Space Partition and Charge Distribution in Multi-Modular Metal–Organic Frameworks, *Angew. Chem., Int. Ed.*, 2022, **61**, e202116064.
26 M. Kang, D. W. Kang and C. S. Hong, Post-synthetic diamine-functionalization of MOF-74 type frameworks for effective carbon dioxide separation, *Dalton Trans.*, 2019, **48**, 2263–2270.
27 P. Horcajada, F. Salles, S. Wuttke, T. Devic, D. Heurtaux, G. Maurin, *et al.*, How Linker's Modification Controls Swelling Properties of Highly Flexible Iron(III) Dicarboxylates MIL-88, *J. Am. Chem. Soc.*, 2011, **133**, 17839–17847.
28 Y. Chen, H. Xie, Y. Zhong, F. Sha, K. O. Kirlikovali, X. Wang, C. Zhang, Z. Li and O. K. Farha, Programmable Water Sorption through Linker Installation into a Zirconium

Metal-Organic Framework, *J. Am. Chem. Soc.*, 2024, **146**, 11202–11210.

29 Z. S. Wang, X. W. Zhang, K. Zheng, X. X. Chen, D. D. Zhou and J. P. Zhang, A topology approach to overcome the pore size/volume trade-offs for autonomous indoor humidity control, *Sci. China Chem.*, 2024, **67**, 2968–2974.

30 W. W. He, G. S. Yang, Y. J. Tang, S. L. Li, S. R. Zhang, Z. M. Su and Y. Q. Lan, Phenyl Groups Result in the Highest Benzene Storage and Most Efficient Desulfurization in a Series of Isostructural Metal-Organic Frameworks, *Chem. Eur. J.*, 2015, **21**, 9784–9789.

31 L. H. Xie, X. M. Liu, T. He and J. R. Li, Metal-Organic Frameworks for the Capture of Trace Aromatic Volatile Organic Compounds, *Chem*, 2018, **4**, 1911–1927.

32 J. Yuan, X. Liu, M. Li and H. Wang, Design of nanoporous materials for trace removal of benzene through high throughput screening, *Sep. Purif. Technol.*, 2023, **324**, 124558.

33 Y. Han, Y. Chen, Y. Ma, J. Bailey, Z. Wang, D. Lee, *et al.*, Control of the pore chemistry in metal-organic frameworks for efficient adsorption of benzene and separation of benzene/cyclohexane, *Chem*, 2023, **9**, 739–754.

34 L. Hu, W. Wang, X. Miao, M. Hu, D. Luo, W. Wu, D. Lin and K. Yang, A novel Al-based MOF with straight channel and pocket pore structure for trace benzene adsorption and benzene/cyclohexane separation, *Chem. Eng. J.*, 2024, **499**, 156376.

35 L. Hu, W. Wu, L. Gong, H. Zhu, L. Jiang, M. Hu, D. Lin and K. Yang, A Novel Aluminum-Based Metal-Organic Framework with Uniform Micropores for Trace BTEX Adsorption, *Angew. Chem., Int. Ed.*, 2023, **62**, e202215296.

36 Y. Z. Zhang, X. D. Zhang, Y. K. Zhang, F. T. Wang, L. l. Geng, H. Hu, *et al.*, Linker engineering in mixed-ligand metal-organic frameworks for simultaneously enhanced benzene adsorption and benzene/cyclohexane separation, *Inorg. Chem. Front.*, 2024, **11**, 8101–8109.

37 Z. Chen, P. Fang, J. Li, X. Han, W. Huang, W. Cui, *et al.*, Rapid extraction of trace benzene by a crown-ether-based metal-organic framework, *Natl. Sci. Rev.*, 2024, **11**, nwae342.

38 L. K. Macreadie, E. J. Mensforth, R. Babarao, K. Konstas, S. G. Telfer, C. M. Doherty, J. Tsanaktsidis, S. R. Batten and M. R. Hill, CUB-5: A Contoured Aliphatic Pore Environment in a Cubic Framework with Potential for Benzene Separation Applications, *J. Am. Chem. Soc.*, 2019, **141**, 3828–3832.

39 J. Chang, F. Chen, H. Li, J. Suo, H. Zheng, J. Zhang, *et al.*, Three-dimensional covalent organic frameworks with nia nets for efficient separation of benzene/cyclohexane mixtures, *Nat. Commun.*, 2024, **15**, 813.

40 C. X. Ren, L. X. Cai, C. Chen, B. Tan, Y. J. Zhang and J. Zhang, π-Conjugation-directed highly selective adsorption of benzene over cyclohexane, *J. Mater. Chem. A*, 2014, **2**, 9015–9019.

41 S. Grimme, J. Antony, S. Ehrlich and H. Krieg, A consistent and accurate ab initio parametrization of density functional dispersion correction (DFT-D) for the 94 elements H-Pu, *J. Chem. Phys.*, 2010, **132**, 154104.

42 T. D. Kühne, M. Iannuzzi, M. Del Ben, V. V. Rybkin, P. Seewald, F. Stein, *et al.*, CP2K: An electronic structure and molecular dynamics software package-Quickstep: Efficient and accurate electronic structure calculations, *J. Chem. Phys.*, 2020, **152**, 194103.

43 J. VandeVondele and J. Hutter, An efficient orbital transformation method for electronic structure calculations, *J. Chem. Phys.*, 2003, **118**, 4365–4369.

44 (*a*) G. Liang D.-J. Chen Z.-J. Long H. Zhuo X.-F. Zhong X.-H. Chen H.-Y. Shao Z.-W. Mo and X.-M. Chen, CCDC 2424097, Experimental Crystal Structure Determination, 2025, DOI: **10.5517/ccdc.csd.cc2mcgp5**; (*b*) G. Liang D.-J. Chen Z.-J. Long H. Zhuo X.-F. Zhong X.-H. Chen H.-Y. Shao Z.-W. Mo and X.-M. Chen, CCDC 2424098, Experimental Crystal Structure Determination, 2025, DOI: **10.5517/ccdc.csd.cc2mcgq6**; (*c*) G. Liang D.-J. Chen Z.-J. Long H. Zhuo X.-F. Zhong X.-H. Chen H.-Y. Shao Z.-W. Mo and X.-M. Chen, CCDC 2424099, Experimental Crystal Structure Determination, 2025, DOI: **10.5517/ccdc.csd.cc2mcgr7**; (*d*) G. Liang D.-J. Chen Z.-J. Long H. Zhuo X.-F. Zhong X.-H. Chen H.-Y. Shao Z.-W. Mo and X.-M. Chen, CCDC 2424100, Experimental Crystal Structure Determination, 2025, DOI: **10.5517/ccdc.csd.cc2mcgs8**; (*e*) G. Liang D.-J. Chen Z.-J. Long H. Zhuo X.-F. Zhong X.-H. Chen H.-Y. Shao Z.-W. Mo and X.-M. Chen, CCDC 2424101, Experimental Crystal Structure Determination, 2025, DOI: **10.5517/ccdc.csd.cc2mcgt9**; (*f*) G. Liang D.-J. Chen Z.-J. Long H. Zhuo X.-F. Zhong X.-H. Chen H.-Y. Shao Z.-W. Mo and X.-M. Chen, CCDC 2424102, Experimental Crystal Structure Determination, 2025, DOI: **10.5517/ccdc.csd.cc2mcgvb**; (*g*) G. Liang D.-J. Chen Z.-J. Long H. Zhuo X.-F. Zhong X.-H. Chen H.-Y. Shao Z.-W. Mo and X.-M. Chen, CCDC 2424103, Experimental Crystal Structure Determination, 2025, DOI: **10.5517/ccdc.csd.cc2mcgwc**; (*h*) G. Liang D.-J. Chen Z.-J. Long H. Zhuo X.-F. Zhong X.-H. Chen H.-Y. Shao Z.-W. Mo and X.-M. Chen, CCDC 2424104, Experimental Crystal Structure Determination, 2025, DOI: **10.5517/ccdc.csd.cc2mcgxd**; (*i*) G. Liang D.-J. Chen Z.-J. Long H. Zhuo X.-F. Zhong X.-H. Chen H.-Y. Shao Z.-W. Mo and X.-M. Chen, CCDC 2424105, Experimental Crystal Structure Determination, 2025, DOI: **10.5517/ccdc.csd.cc2mcgyf**; (*j*) G. Liang D.-J. Chen Z.-J. Long H. Zhuo X.-F. Zhong X.-H. Chen H.-Y. Shao Z.-W. Mo and X.-M. Chen, CCDC 2424106, Experimental Crystal Structure Determination, 2025, DOI: **10.5517/ccdc.csd.cc2mcgzg**.